This is the Pre-Published Version.

This version of the article has been accepted for publication, after peer review (when applicable) and is subject to Springer Nature's AM terms of use(https://www.springernature.com/gp/open-research/policies/accepted-manuscript-terms), but is not the Version of Record and does not reflect post-acceptance improvements, or any corrections. The Version of Record is available online at: http://dx.doi.org/10.1007/s10800-018-1212-4.

Boosting the lithium-ion storage performance of dense $MnCO_3$ microsphere anodes via Sb-substitution and construction of neural-like carbon nanotube networks

Hao Lu[1], Yanwu Fang[1], Jike Yang[1], Mingtong Yang[1], Qingchuan Du[1], Ling Ba[1]i, Kang Xiao[1], Titus Masese[2], Xusheng Yang[3], Zhen-Dong Huang[1,*] & Yanwen Ma[1,*]

[1]*Key Laboratory for Organic Electronics and Information Displays & Jiangsu Key Laboratory for Biosensors, Institute of Advanced Materials (IAM), Jiangsu National Synergetic Innovation Center for Advanced Materials (SICAM), Nanjing University of Posts & Telecommunications, 9 Wenyuan Road, Nanjing, 210023, China*

[2]*Research Institute of Electrochemical Energy, National Institute of Advanced Industrial Science and Technology (AIST), Ikeda, Osaka, 563-8577, Japan*

[3]*Advanced Manufacturing Technology Research Centre, Department of Industrial and Systems Engineering, The Hong Kong Polytechnic University, Hung Hom, Kowloon, Hong Kong, China*

Corresponding authors:

Zhen-Dong Huang: iamzdhuang@njupt.edu.cn; hzd0506127@gmail.com

Yanwen Ma: iamywma@njupt.edu.cn

Abstract

To boost the electrochemical performance of $MnCO_3$ (MC) microspheres, binary $Sb_xMn_{1-x}CO_3$ ($x = 1/3$, $1/2$ and $2/3$) microspheres, labeled SMC-12, SMC-11 and SMC-21, respectively, were prepared using a solvothermal method. A 3D conductive network of carbon nanotubes (CNT) was also successfully built from the inside to the surface of the SMC-12 microspheres to promote electronic and ionic transportation. As observed, the microspheres of SMC-12 were larger and had a more uniform distribution compared with pure MC, SMC-11 and SMC-21. Profiting from the introduction of neural-like CNTs networks, the electrochemical performance and the utility of the SMC-12 microspheres (approximately 3.5–7 μm in diameter) were remarkably improved. The obtained CNTs@SMC-12 composite anode delivered 1066 and 572 mAh g^{-1} at current densities of 500 and 5000 mAg^{-1} after 200 cycles, respectively, which were much higher than the 737 and 297 mAh g^{-1} of bare SMC-12.

Keywords: Lithium ion batteries; Anode materials; Carbon nanotube; Carbonates microspheres

Introduction

In a future artificial intelligence (AI) human society, lithium-ion batteries (LIBs) with superior lithium-ion storage performance will be highly important for powering smart and portable AI electronic facilities, including various types of intelligent robots, electric vehicles (EV) and smartphones [1, 2]. However, the limited energy densities of conventional LIBs built with graphite as the anode and lithium cobalt oxide as the cathode cannot satisfy the ever-increasing application requirements [3, 4]. Recently, various nanostructured anode materials, including silicon/carbon nanocomposites [5-7], metal oxides [8-16], sulfides [17-20], and carbonates [21-31], have been developed as promising candidates. Among these, microscale spherical carbonates have gained more attention due to their high volumetric energy density and suppressed side-reactions resulting from the high tap density and low exposed surface area [21-25]. There are always two sides to everything: the dense structure and low exposed surface area of active microsphere materials always result in slow (de-) intercalation kinetics for Li^+, a much longer charge transfer distance, a much larger charge transfer resistance and worse structure stability compared to those of the nanosized materials, and these factors are responsible for the degraded lithium-ion storage performance with the increment in particle size for the reported $MnCO_3$ spheres [21].

To overcome these limitations, carbonate microspheres doped by dopants with different porous and hierarchical structures were recently designed and developed [21-25]. As reported, the doped binary $Mn_{1-X}Co_XCO_3$ normally delivered exceptionally superior lithium-ion storage properties compared to those of pure $MnCO_3$ and $CoCO_3$ [24, 27]. It is also interesting to note that two-dimensional reduced graphene oxide (RGO) has been used a popular outer coating to wrap carbonate spheres for building an in vitro conductive network; unfortunately, the additional reduction process that is required to reduce GO to RGO might destroy the carbonate structure [26-29]. Zero-dimensional carbon nanoparticles have also been used to improve the conductivity and alleviate the volume change of electrode during charge/discharge; however, a large number of carbon nanoparticles is required to form an effective 3D conductive network [32]. Similar to 2D RGO and 0D carbon nanoparticles, 1D carbon nanotubes (CNTs) are common conductive additives for both cathodes and anodes; however, in most cases, CNTs were used as outer surface conductive additives, such as RGO and amorphous carbon [31, 32], but they did not take advantage of one-dimensional conductive characteristics. Moreover, no additional reduction process is required after the in situ preparation of carbonate microspheres with CNTs networks. This advantage will help maintain the structure and other properties of carbonate compounds, which is one of the advantages of using 1D CNTs as conductive additives.

Based on these discussions, binary $Sb_{1/3}Mn_{2/3}CO_3$ microspheres with an in vivo carbon nanotube “neural” network were designed and successfully built from the inside to the surface of dense SMC-12 microspheres to improve the electronic conductivity and create lithium ion transfer channels from core to shell during the (dis)charge process as high-energy-density anode materials. Electrochemical measurements indicated that the as-prepared $Sb_{1/3}Mn_{2/3}CO_3$ (SMC-12) showed better lithium-ion storage performance than pure $MnCO_3$, binary $Sb_{1/2}Mn_{1/2}CO_3$ (SMC-11) and $Sb_{2/3}Mn_{1/3}CO_3$ (SMC-21). As desired, the as-prepared CNTs/SMC-12 composite microspheres exhibited both smaller contact and charge transfer resistances and, in turn, achieved excellent electrochemical performance. After 200 cycles, the charge capacity of CNTs/SMC-12 composite electrodes retained 1066 and 572 mAh g^{-1} at 500 and 5000 mAg^{-1}, respectively, which were much higher than the 737 and 297 mAh g^{-1} of bare SMC-12 microspheres.

Experimental

Preparation of SMC microspheres

SMC microspheres were prepared by following a urea-assisted solvothermal method. Ethylene glycol (EG) was used as the solvent. $C_6H_9O_6Sb$ and $C_4H_6O_4Mn{\cdot}4H_2O$ were chosen as antimony and manganese sources. Urea was used as both the precipitator and the complexing agent. At the beginning of a typical procedure, 0.0033 mol $C_6H_9O_6Sb$, 0.0067 mol $C_4H_6O_4Mn{\cdot}4H_2O$ and 0.05 mol urea were successively dissolved in 70 ml of EG solvent under continuous magnetic stirring. After stirring for 120 min at room temperature, the obtained clear solution was transferred and sealed in a 100-ml Teflon-lined stainless autoclave. After 10 h of solvothermal reaction in a blowing drying furnace preheated to 160 °C, the autoclave was cooled to room temperature. The brown product was washed with water and ethanol successively three times. Then, the final SMC-12 was collected after drying in a vacuum oven at 60 °C for 24 h. Pure $MnCO_3$, other binary carbonates SMC-11 and SMC-21 were prepared by following the same procedure with the same molar ratios between metal ions and urea.

Preparation of SMC-12@CNT hybrid microspheres

In order to successfully obtain SMC-12 with a CNTs “neural”-like network, it is important to cut the MWCNTs (50–70 nm in diameter, 10–15 μm in length) to a proper length, to modify the surface condition of the applied MWCNTs to ensure their dispersivity. Therefore, in this work, the received MWCNTs were first treated with a mixed solution of thick sulfuric acid and hydrogen peroxide in a volumetric ratio of 3:1 at 90 °C. After 24 h of acidification treatment, the CNTs acid solution was dispersed into 1000 ml of distilled water under magnetic stirring followed by 15 min of ultrasonication treatment. Then, the cut and acidified CNTs were collected via vacuum filtration and washed with water and ethanol successively three times. Subsequently, the acidified CNTs were dried at 70 °C for 24 h and labeled ACNTs. To further improve the dispersivity of ACNTs in the EG solution, polyvinylpyrrolidone (PVP) with a mass ratio of 1:20 to ACNTs were used as the surfactant to modify the surface of ACNTs. Then, 0.062 g of ACNTs and 0.0031 g of PVP were dispersed and dissolved in 70 ml of EG. After 1 h ultrasonication treatment, a uniform ACNT dispersion is finally obtain. Subsequently, 0.0033 mol $C_6H_9O_6Sb$, 0.0067 mol $C_4H_6O_4Mn\cdot4H_2O$ and 0.05 mol urea were successively dissolved in the obtained ACNT EG dispersion to form a final mixed solution under continuous magnetic stirring at room temperature. The following solvothermal and product collection processes were the same as that used to prepare the SMC microspheres mentioned above. Finally, the desired SMC-12@CNT hybrid microspheres were obtained for physical and electrochemical characterizations.

Characterizations

The crystal structures of the as-prepared SMC and SMC@CNT hybrids were characterized by X-ray diffraction (XRD) (X-ray diffractometer, Bruker D8 Advance A25) using Cu Kα radiation ($\lambda = 1.54051$ Å). The diffraction patterns were recorded in a 2θ range of 20–70° with a step size of 0.02°. The morphologies of the as-prepared SMC and SMC@CNT hybrids were observed using field emission scanning electron microscopy (FE-SEM, Hitachi S-4800) at an acceleration voltage of 3 kV. TG/DSC measurement was conducted by differential scanning calorimetry (DSC; NTEZSCH, Germany, STA 409) in the air at a scan rate of 10 °C min^{-1} from room temperature to 800 °C to investigate the fraction of CNTs within the final products. The fraction of ACNT within the SMC-12@CNTs hybrids is estimated by comparing the mass loss during TG measurement with pure SMC-12. The loss of moisture (I), the loss of CO_2 during the decomposition of SMC to form $Sb_{2/3}Mn_{4/3}O_3$ (II, 31.2%) and the loss of O during the continuously high temperature annealing of $Sb_{2/3}Mn_{4/3}O_3$ to form $SbMn_2O_4$ (III, 2.6%) should be responsible for the mass loss during the annealing process of SMC-12. The additional mass loss of SMC-12@CNTs (IV) should be resulted from the burning of ACNT.

To investigate the electrochemical performance of as-prepared SMC and SMC-12@CNTs hybrids, the composite electrodes of the final product were prepared by coating the uniform slurry mixed with acetylene black (AB) and polyvinylidene fluoride (PVDF) (active materials: AB: PVDF = 80: 10: 10) on copper foil. After drying at 70 °C for 3 h in air followed by 8 h under vacuum in drying boxes, the electrodes were then pressed and punched into 13 mm (in diameter) disks. The average mass loading was approximately 1 mg cm^{-2}. Two-electrode lithium-ion batteries were assembled in an ultrapure Ar-gas filled glove box to investigate the lithium-ion storage performance of the SMC and SMC-12@CNTs. The electrolyte used was a 1 mol L^{-1} $LiPF_6$ in ethylene carbonate (EC) + dimethyl carbonate (DMC) at a volume ratio of 1:1. Lithium discs were used as counter and reference electrodes. Cyclic voltammetry (CV) and galvanostatic charge and discharge measurements were carried out in a voltage range of 0.01 to 3 V vs. Li/Li^+ at a current density ranging from 0.25 to 5 Ag^{-1}, respectively. Electrochemical impedance spectroscopy (EIS) was carried out in a frequency range of 0.01 Hz to 100 kHz, and the perturbation amplitude was controlled at 5 mV. A Biologic VMP3 multi-channel electrochemical workstation was used to record the CV and EIS results. The galvanostatic charge/discharge tests were performed on a battery testing system (CT2001A, Wuhan Land). The aged cells were discharged/charged within the voltage window of 0.01 to 3.0 V at current densities from 500 mAg^{-1} to 5 Ag^{-1} under constant current mode.

Results and discussion

Crystal structure and morphology of as-prepared unitary and binary carbonates

The obtained XRD and FE-SEM analysis results are shown in Figs. 1 and 2. As shown in Fig. 1a, the observed XRD patterns were consistent with the standard pattern based on PDF#44-1472 indexed to the rhombohedral space group R-3C (167). No crystalline impurity phase was found in the observed XRD patterns. The peak intensity ratio between the peaks corresponding to the crystal face (104) and (012), namely, $I_{(104)}/I_{(012)}$, for the obtained MC microspheres was approximately 4.1, close to 4.3 for the standard patterns. It is also interesting to note that the ratio of $I_{(104)}/I_{(012)}$ increased almost linearly from 4.1 to 7.48 with the increment of the fraction of the substituted Sb to Mn into MC, as shown in Fig. 1b. This observation indicated that as increasing numbers of Mn ions were substituted by Sb ions, the distortion of the unit lattice of MC become more profound. In particular, when the substitution fraction was over 50%, the XRD peak intensity became progressively weaker, as observed in Fig. 1a. However, a smooth XRD pattern SMC-12 with sharp peaks and distinguishable dual peaks corresponding to the crystal face of (018) and (016) was seen, indicating that a small amount of doping modified the crystal structure of MC.

The overall view of as-prepared carbonates microspheres is shown in Fig. 2. As observed from the SEM image shown in Fig. 2a, the size of as-prepared MC microspheres ranged from 2 to 7 μm, of which spheres of 5–7 μm were ~ 10%, 2–5 μm were ~ 65% and < 2 μm were ~ 25%. Compared to MC, the size distribution of SMC-12 spheres became narrow, primarily 3.5–7 μm. Among these, 6–7 μm was ~ 63%, 2–4 μm was ~ 22% and < 2 μm was ~ 15%, as seen in Fig. 2b. This observation indicated that a certain amount of Sb-substitution was helpful to obtaining large but uniform SMC microspheres. However, when the substitution fraction of Mn ions with Sb was up to or over 50%, the uniformity of the obtained SMC-11 and SMC-12 became worse than that of MC; more than 50% of non-holonomic sphere particles were found from the SEM images provided in Fig. 2c, d. Especially, more SMC-11 particle with a large size than 7 μm can be found from Fig. 2c.

Morphology and crystal structure of as-prepared SMC-12@CNTs hybrids

To enhance the electron and ion transportation within and between the carbonates SMC-12 microspheres, the ACNT were successfully incorporated inside and outside the SMC-12 microspheres. As shown in Fig. 3a, the size of SMC-12@CNT hybrid microspheres were similar with the neat SMC-12. Most of the spheres were uniformly coated with ACNT networks, while the length and the arrangement direction of ACNTs observed from high-magnification SEM image shown in Fig. 3b indicates that ACNTs were embedded inside the SMC-12 microspheres. A three-dimensional (3D) CNTs “neural”-like network was formed in the SMC-12@CNTs hybrids, which facilitated the transportation of Li-ions and electrons and in turn, contributed to the much-improved lithium-ion storage properties discussed below. The XRD pattern provided in Fig. 3c showed that the in situ incorporation process of CNTs network did not affect the formation of the highly crystalline SMC-12. Moreover, the ACNT content within SMC-12@CNTs hybrids was estimated by using the TG analysis results shown in Fig. 3d. The estimated content of ACNT is approximately 5.2 wt%, which is close to the theoretical ACNT content of 4.5 wt%.

The electrochemical performance of the obtained carbonates and SMC-12@CNTs hybrids

Figure 4 shows the electrochemical performance of the obtained MC, SMC-12, SMC-11 and SMC-21 at the current density of 1 Ag^{-1}. As shown in Fig. 4a, the as-prepared SMC-12 with a larger and uniform particle size exhibited much higher capacity and better cyclic stability than SMC-21, SMC-11 or MC. Initially, the discharge/charge capacity decreased gradually from 338.2/321.6 to 281.3/277.9 mAh g^{-1}, and it then grew slowly to 435.1/434.2 mAh g^{-1} at the 160th cycle at 1 Ag^{-1}. A similar phenomenon was also observed for the cyclic performance of SMC-21. The gradual increment of specific capacity was due to the gradual activation of the large active microsphere particles, namely, the crescent utility of effective active materials. The much longer discharge plateau at 0.32 V than those of MC and SMC-11 further confirmed the better electrochemical activity of SMC-12, as shown in the discharge profiles in Fig. 4b. The larger size of particle and larger distortion of crystal structure should be responsible to the worse lithium ion storage performance of SMC-11 than SMC-12 and SMC-21.

Figure 5 shows the electrochemical performance of as-prepared SMC-12 and SMC-12@CNTs hybrids. As shown in Fig. 5a, b, the cyclic performance at 0.5 and 5 Ag^{-1} indicated that SMC-12@CNTs hybrids exhibited much better cyclic and rate capability than SMC-12 microspheres. The evolution of room temperature from day to night should be mainly accounted for by the fluctuation of the long-term cyclic testing results, especially at a relatively low current density. After being cycled at 0.5 Ag^{-1} for 160 cycles, the discharge/charge specific capacity of SMC-12@CNTs gradually grew to 1079.6/1065.7 mAh g^{-1}, which was much larger than the 724.6/736.8 mAh g^{-1} of bare SMC-12. In particular, at the much higher current density of 5 Ag^{-1}, the discharge/charge specific capacity of SMC-12@CNTs retained 575.8/571.9 mAh g^{-1} after 160 cycles, much greater than the 301.8/296.5 mAhg-1 of bare SMC-12. The typical dis(charge) profiles of both SMC-12 and SMC-12@CNTs hybrids at 160 cycles under a current density of 0.5 and 5 Ag^{-1} are displayed in Fig. 5c, d, respectively. Based on the morphology and the electrochemical testing results, the successful construction of the desired 3D CNTs “neural”-like network were responsible for the exceptional rate and cyclic performance of SMC-12@CNTs hybrids. Greater oxidation and larger reduction peak current densities of SMC-12@CNTs were observed from the CV curves shown in Fig. 5e. Smaller contact resistance and charge transfer resistance, responsible for the much superior lithium-ion storage performance of SMC-12@CNTs hybrids, could be observed from the EIS testing results given in Fig. 5f. The much-reduced inner resistance further confirmed the successful formation of the desired 3D CNTs “neural”-like conductive networks. Furthermore, it is exciting to find that the electrochemical performance achieved by as-prepared SMC-12, SMC-12@CNT hybrid microsphere anode materials were exceptional and were much greater than those of most of the reported similar spherical carbonate anode materials. As displayed in Table 1, present Sb-substituted $MnCO_3$, namely, SMC-12, delivered a much better cyclic performance and rate capability than did the reported $MnCO_3$ with similar or even smaller particle sizes [21]. Moreover, the obtained MC-12@CNT hybrid exhibited comparable or even better electrochemical performance than did nanostructured carbonates with a smaller size or modified with graphene/CNT [24, 25, 27, 30].

Conclusions

In this study, the structure, morphology and electrochemical performance of $MnCO_3$ microspheres were remarkably improved through antimony (Sb) substitution and the introduction of 3D CNTs “neural”-like conductive networks. The $MnCO_3$ and Sb-substituted binary $Sb_xMn_{1-x}CO_3$ microspheres were successfully assembled by following a urea-assisted solvothermal reaction. XRD and SEM analysis indicated that a small amount of Sb-substitution was helpful to obtain carbonate microspheres with a uniform size distribution and well-developed crystal structures. Consequently, the as-prepared SMC-12 showed both larger and uniform size distribution and, in turn, resulted in better lithium-ion storage performance than those of pure $MnCO_3$, binary carbonates SMC-11 or SMC-21. Furthermore, in vivo 3D carbon nanotube “neural”-like conductive networks were designed to solve the problems limiting the performance of high tap density micron-size spherical SMC-12. With the successful construction of 3D “neural”-like CNTs conductive networks inside and outside the SMC-12 microsphere, the rate and cyclic performance, as well as the utility of the larger SMC-12 microspheres, were markedly improved due to the greatly enhanced electronic and ionic transportation from core to shell and the partial remission of inner stress during the (dis)charge process. As a result, the charge capacity of CNTs/SMC-12 composite microspheres retained 1066 and 572 mAh g^{-1} after 200 cycles at the current density of 500 and 5000 mAg^{-1}, respectively, much larger than the 737 and 297 mAh g^{-1} of bare SMC-12 microspheres.

Acknowledgements

This work was supported by National Natural Science Foundation of China (51402155), Priority Academic Program Development of Jiangsu Higher Education Institutions (PAPD) (YX03002), Jiangsu National Synergistic Innovation Center for Advanced Materials (SICAM), Foundation of NJUPT (NY217077) and PolyU Start-up Fund for New Recruits (No. 1-ZE8R).

References:

1. Sun YM, Liu N, Cui Y (2016) Promises and challenges of nanomaterials for lithium based rechargeable batteries. Nat Energy 1:16071

2. Yuan CZ, Wu HB, Xie Y, Lou XW (2014) Mixed transition-metal oxides: design, synthesis, and energy-related applications. Angew Chem Int Ed 53:1488–1504

3. Whittingham MS (2014) Ultimate limits to intercalation reactions for lithium batteries. Chem Rev 114(23):11414–11443

4. Yang FH, Yu F, Zhang ZA, Zhang K, Lai YQ, Li J (2016) Bismuth nanoparticles embedded in carbon spheres as anode materials for sodium/lithium-ion batteries. Chem Eur J 22:2333–2338

5. Xu ZL, Cao K, Abouali S, Garakani MA, Huang JQ, Huang JQ, Heidari EK, Wang HT, Kim JK (2016) Study of lithiation mechanisms of high performance carbon-coated Si anodes by in-situ microscopy. Energy Storage Mater 3:45–54

6. Huang ZD, Zhang K, Zhang TT, Liu RQ, Lin XJ, Li Y, Feng XM, Mei QB, Masese T, Ma YW, Huang W (2016) Binder-free graphene/carbon nanotube/silicon hybrid grid as freestanding anode for high capacity lithium ion batteries. Compos Part A 84:386–392

7. Li S, Qin XY, Zhang HR, Wu JX, He YB, Li BH, Kang FY (2014) Silicon/carbon composite microspheres with hierarchical core–shell structure as anode for lithium ion batteries. Electrochem Commun 49:98–102

8. Miao C, Liu M, He YB, Qin XY, Tang LK, Huang B, Li R, Li BH, Kang FY (2016) Monodispersed SnO_2 nanospheres embedded in framework of graphene and porous carbon as anode for lithium ion batteries. Energy Storage Mater 3:98–105

9. Huang ZD, Zhang K, Zhang TT, Yang XS, Liu RQ, Li Y, Lin XJ, Feng XM, Ma YW, Huang W (2016) Hierarchical $NiCoO_2$ mesoporous microspheres as anode for lithium ion batteries with superior rate capability. Energy Storage Mater 3:36–44

10. Cui ZH, Li CL, Yu PF, Yang MH, Guo XX, Yin CL (2015) Reaction pathway and wiring network dependent Li/Na storage of micro-sized conversion anode with mesoporosity and metallic conductivity. J Mater Chem A 3:509–514

11. Huang ZD, Zhang TT, Lu H, Masese T, Yamamoto K, Liu RQ, Lin XJ, Feng XM, Liu XM, Wang D, Uchimoto Y, Ma YW (2017) Grain-boundary-rich mesoporous $NiTiO_3$ micro prism as high tap-density, super rate and long life anode for sodium and lithium ion batteries. Energy Storage Mater. https://doi.org/10.1016/j.ensm.2017.08.012

12. Fang W, Zhang NQ, Fan LS, Sun KN (2016) Bi_2O_3 nanoparticles encapsulated by three dimensional porous nitrogen-doped graphene for high-rate lithium ion batteries. J Power Sources 333:30–36

13. Hou LR, Lian L, Zhang LH, Pang G, Yuan CZ, Zhang XG (2014) Self-sacrifi ce template fabrication of hierarchical mesoporous Bi-component-active $ZnO/ZnFe_2O_4$ submicrocubes as superior anode towards high-performance lithium-ion battery. Adv Funct Mater. https://doi.org/10.1002/adfm.201402827

14. Zhang LH, Zhu SQ, Cao H, Pang G, Lin JD, Hou LR, Yuan CZ (2015) Ultrafast spray pyrolysis fabrication of a nanophase $ZnMn_2O_4$ anode towards high-performance Li-ion batteries. RSC Adv 5:13667–13673

15. Guo LY, Ru Q, Song X, Hu SJ, Mo YD (2015) Pineapple-shaped $ZnCo_2O_4$ microspheres as anode materials for lithium ion batteries with prominent rate performance. J Mater Chem 3:8683–8692

16. Zhu YQ, Cao CB, Zhang JT, Xu XY (2015) Two-dimensional ultrathin $ZnCo_2O_4$ nanosheets: general formation and lithium storage application. J Mater Chem A 3:9556–9564

17. AbdelHamid AA, Yang XF, Yang JH, Chen XJ, Ying JY (2016) Graphene-wrapped nickel sulfide nanoprisms with improved performance for Li-ion battery anodes and supercapacitors. Nano Energy 26:425–437

18. Chen B, Liu EZ, Cao TT, He F, Shi CS, He CN, Ma LY, Li QY, Li JJ, Zhao NQ (2017) Controllable graphene incorporation and defect engineering in MoS_2-TiO_2 based composites: Towards high-performance lithium-ion batteries anode materials. Nano Energy 33:247–256

19. Zhou YL, Yan D, Xu HY, Feng JK, Jiang XL, Yue J, Yang J, Qian YT (2015) Hollow nanospheres of mesoporous Co_9S_8 as a high-capacity and long-life anode for advanced lithium ion batteries. Nano Energy 12:528–537

20. Liu Y, Shi YD, Liu X, Li HX (2017) A facile solvothermal approach of novel Bi_2S_3/TiO_2/RGO composites with excellent visible light degradation activity for methylene blue. Appl Surf Sci 396:58–66

21. Xiao L, Wang SY, Wang YF, Meng W, Deng BH, Qu DY, Xie ZZ, Liu JP (2016) High capacity and self-stabilized manganese carbonate microspheres as anode material for lithium ion batteries. ACS Appl Mater Interfaces 8(38):25369–25378

22. Lee H-K, Sakemi D, Selyanchyn R, Lee CG, Lee SW (2014) Titania nanocoating on $MnCO_3$ microspheres via liquid-phase deposition for fabrication of template-assisted core-shell-and hollow-structured composites. ACS Appl Mater Interfaces 6(1):57–64

23. Zhong YR, Yang M, Zhou XL, Luo YT, Wei JM, Zhou Z (2015) Orderly packed anodes for high-power lithium-ion batteries with super-long cycle life: rational design of $MnCO_3$/large-area graphene composites. Adv Mater 27(5):806–812

24. Yin JJ, Ding ZJ, Lei DL, Tang LK, Deng JJ, Li BH, He YB (2017) Zn-substituted $CoCO_3$ embedded in carbon nanotubes network as high performance anode for lithium-ion batteries. J Alloy Compd 712:605–612

25. Kang W, Yu DYW, Li W, Zhang Z, Yang X, Ng T-W, Zou R, Tang Y, Zhang W, Lee C-S (2015) Nanostructured porous manganese carbonate spheres with capacitive effects on the high lithium storage capability. Nanoscale 7(22):10146–10151

26. Zhou L, Kong X, Gao M, Lian F, Li B, Zhou Z, Cao H (2014) Hydrothermal fabrication of $MnCO_3$@rGO composite as an anode material for high-performance lithium-ion batteries. Inorg Chem 53(17):9228–9234

27. Zhang R, Huang XX, Wang D, Hoang TKA, Yang Y, Duan XM, Chen P, Qin LC, Wen GW (2018) Single-phase mixed transition metal carbonate encapsulated by graphene: facile synthesis and improved lithium storage properties. Adv Funct Mater. https://doi.org/10.1002/adfm.201705817

28. Zhao S, Feng F, Yu F, Shen Q (2015) Flower-to-petal structural conversion and enhanced interfacial storage capability of hydrothermally crystallized $MnCO_3$ via the in-situ mixing of graphene oxide. J Mater Chem A 3(47):24095–24102

29. Yao B, Ding ZJ, Feng XY, Yin LW, Shen Q, Shi YC, Zhang JX (2014) Enhanced rate and cycling performance of $FeCO_3$/graphene composite for high energy Li ion battery anodes. Electrochim Acta 148:283–290

30. Zhang L, Mei T, Wang X, Wang J, Li J, Xiong W, Chen Y, Hao M (2015) Hierarchical architectured $MnCO_3$ microdumbbells: facile synthesis and enhanced performance for lithium-ion batteries. CrystEngComm 17(33):6450–6455

31. Zhang F, Zhang RH, Liang GM, Feng JK, Lu L, Qian YT (2013) Carboxylated carbon nanotube anchored $MnCO_3$ nanocomposites as anode materials for advanced lithium-ion batteries. Mater Lett 111:165–168

32. Huang ZD, Zhang B, He YB, Oh SW, Yu Y, Kim JK (2012) Addition of silane functionalized carbon nanotubes for improved rate capability of $LiNi_{1/3}Co_{1/3}Mn_{1/3}O_2$ cathodes for lithium ion batteries. J Electrochem Soc 159(12):A2024–A2028

Figure 1

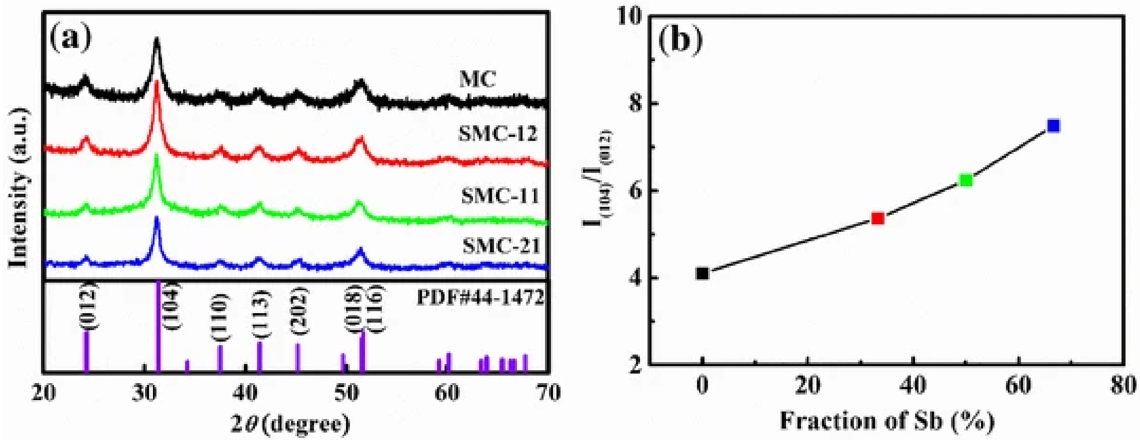

Fig 1 **a** XRD patterns of as-prepared MC, SMC-12, SMC-11, SMC-21 and the standard pattern, **b** the intensity ratio of $I_{(104)}/I_{(012)}$ vs. the substitution fraction of Mn ions with Sb ions.

Figure 2

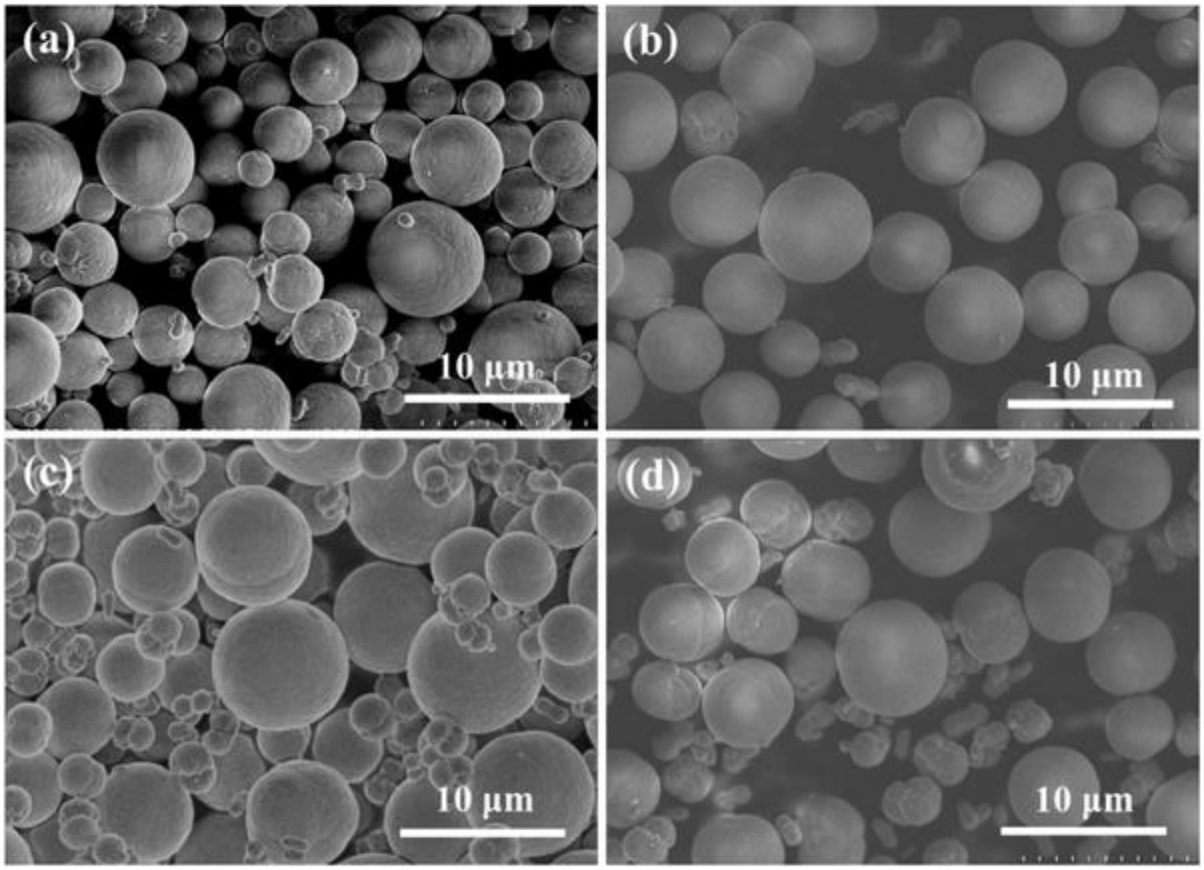

Fig 2 SEM images of as-prepared carbonate microspheres: **a** MC, **b** SMC-12, **c** SMC-11 and **d** SMC-21, respectively.

Figure 3

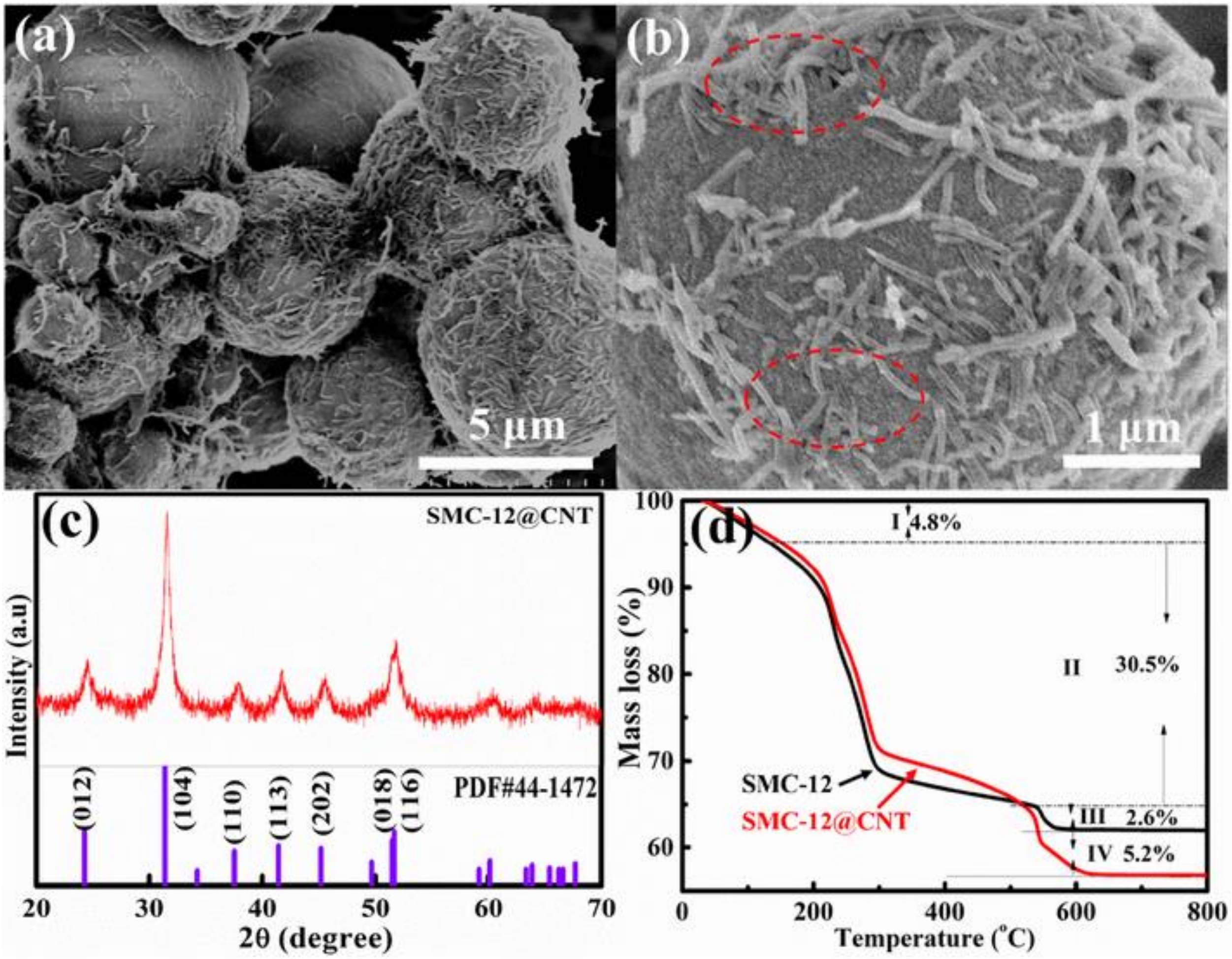

Fig 3 a and **b** SEM images, **c** XRD pattern of the obtained SMC-12@CNTs, **d** TG analysis results of both SMC-12 and SMC-12@CNTs in the air.

Figure 4

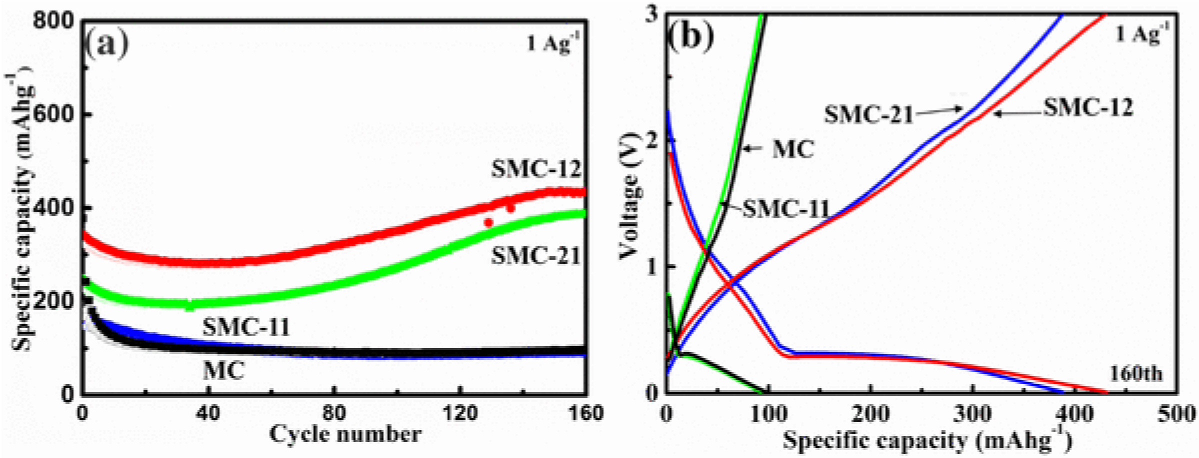

Fig 4 **a** The cyclic performance and **b** the 160th cycle's charge/discharge profiles of as-prepared MC, SMC-12, SMC-11 and SMC-21 at the current density of 1 Ag^{-1}, respectively.

Figure 5

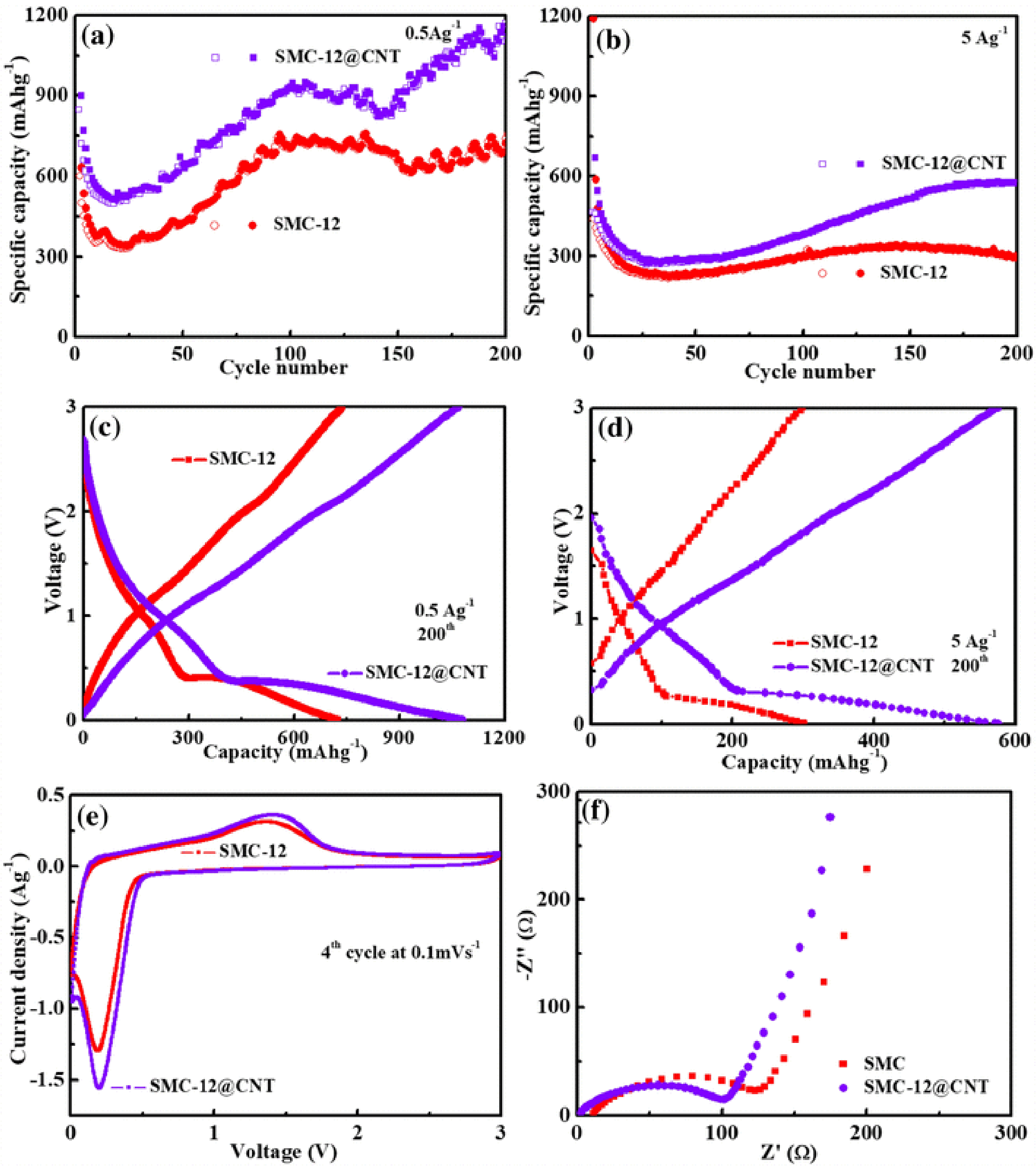

Fig 5 a, b cyclic performance of as-prepared SMC-12 and SMC-12@CNTs hybrids at the current density of 0.5 and 5 Ag^{-1}, respectively; **c, d** the charge/discharge profiles corresponding to the 200th cycle at the current density of 0.5 and 5 Ag^{-1}, **e** CV curve and **f** EIS analysis results of as-prepared SMC-12 and SMC-12@CNTs hybrids, respectively

Table 1 Comprehensive comparison of the present Sb1/3Mn2/3CO3 (SMC-12), SMC-12@CNT hybrid microsphere anode materials with other reported similar spherical carbonate anode materials

No.	Materials and morphology	Secondary particle size (μm)	Retained capacity (mAh g^{-1})	Current density (mAg^{-1})	Cycle number	Refs. no.
1	SMC-12@CNT hybrid microspheres	2–7	1066 572	500 5000	160 160	Present work
	SMC-12	3.5–7	737 297	500 5000	160 160	
2	$MnCO_3$ microspheres	2.6	656.8	100	100	21
		4	573.9	100	100	
		6.9	487.6	100	100	
3	$Zn_{0.12}Co_{0.88}CO_3$/CNT spherical composite	2–4	710	100	50	24
4	Porous $MnCO_3$ spheres	500	1049	1000	200	25
5	$Mn_{0.7}Co_{0.3}CO_3$/RGO	1	1432 900 ~ 500	100 2000 5000	130 1500 200	27
6	Hierarchical $MnCO_3$ microdumbbell	Length: 0.5–1.5; width: 0.3–0.9	775	500	100	30